CELLULAR NEUROSCIENCE

The biophysical, molecular, and anatomical landscape of pigeon CRY4: A candidate light-based quantal magnetosensor

Tobias Hochstoeger[1], Tarek Al Said[2], Dante Maestre[1], Florian Walter[1], Alexandra Vilceanu[1], Miriam Pedron[1], Thomas D. Cushion[1], William Snider[3], Simon Nimpf[1], Gregory Charles Nordmann[1], Lukas Landler[4], Nathaniel Edelman[5], Lennard Kruppa[2], Gerhard Dürnberger[1,6], Karl Mechtler[1,6], Stefan Schuechner[7], Egon Ogris[7], E. Pascal Malkemper[7,8], Stefan Weber[2], Erik Schleicher[2], David A. Keays[1,9,10]*

The biophysical and molecular mechanisms that enable animals to detect magnetic fields are unknown. It has been proposed that birds have a light-dependent magnetic compass that relies on the formation of radical pairs within cryptochrome molecules. Using spectroscopic methods, we show that pigeon cryptochrome clCRY4 is photoreduced efficiently and forms long-lived spin-correlated radical pairs via a tetrad of tryptophan residues. We report that clCRY4 is broadly and stably expressed within the retina but enriched at synapses in the outer plexiform layer in a repetitive manner. A proteomic survey for retinal-specific clCRY4 interactors identified molecules that are involved in receptor signaling, including glutamate receptor–interacting protein 2, which colocalizes with clCRY4. Our data support a model whereby clCRY4 acts as an ultraviolet-blue photoreceptor and/or a light-dependent magnetosensor by modulating glutamatergic synapses between horizontal cells and cones.

INTRODUCTION

The ability to detect magnetic fields is a sensory faculty exploited by a wide array of animals on the planet to aid navigation. This sense is not limited to species that undertake lengthy annual migrations but has also been reported in animals that undertake localized journeys such as bees, newts, bats, mole rats, lobsters, and pigeons (*1*). How these species detect magnetic information and transduce it into a neuronal impulse remains an unresolved question in modern biology. One hypothesis that provides an intellectual framework for tackling the problem is known as the radical pair mechanism (RPM). It predicts that the spin state of light-induced radical pairs is influenced by local magnetic fields, altering the photochemical properties of a receptor protein (*2*, *3*). This hypothesis is supported by evidence showing that the magnetic orientation is dependent on the wavelength of light. Migratory birds require the presence of light in the blue/green spectrum (from 370 to 565 nm) (*4*); newts need blue light (<475 nm) for shoreward orientation (*5*); conditioning of *Drosophila melanogaster* to a magnetic stimulus requires light in the ultraviolet A (UV-A)/blue spectrum (<420 nm) (*6*); and pigeon homing is perturbed by exposure to red light (660 nm) on their outward journey but not green (565 nm) or white light (*7*). Moreover, it has been shown that low-intensity radio-frequency fields (which influence the spins of coupled radical pairs) disrupt magnetic orientation in European robins (*8*, *9*), zebra finches (*10*), rodents (*11*), and cockroaches (*12*).

The cryptochrome family is widely considered to be the best candidate for an RPM-based magnetoreceptor (*2*). Cryptochromes are signaling molecules that are found throughout the animal kingdom that are related to the DNA photolyases and play a key role in circadian regulation (*13*). In *Drosophila*, cryptochromes regulate circadian entrainment by light-dependent interaction with TIMELESS and the E3 ubiquitin ligase JETLAG (*14*), whereas in mice, cryptochromes (CRY1 and CRY2) function as light-independent components of the circadian clock (*15*). The photosensitivity of type 1 invertebrate cryptochromes has been attributed to its cofactor flavin adenine dinucleotide (FAD), which does not appear to bind to type 2 mammalian cryptochromes (*16*, *17*). The latter fact has been a particular issue for the RPM hypothesis as it predicts that long-lived radical pairs are formed when light induces the transfer of electrons to this FAD moiety along a chain of tryptophan residues. Moreover, the primary sensors should be aligned in a meaningful way to provide directional information and be linked to an intracellular signaling mechanism enabling modulation of neuronal activity. Here, we show that CRY4 in pigeon binds FAD, forms long-lived spin-correlated radical pairs, is enriched at synapses in the retina in a stereotypical manner, and interacts with the glutamate receptor–interacting proteins GRIP1/2.

RESULTS

clCRY4 binds FAD, is photoreduced, and undergoes light-induced conformational changes

To determine whether the pigeon cryptochromes bind FAD, we cloned and expressed clCRY1a, clCRY2a, and clCRY4 in insect cells and purified the proteins by affinity and size exclusion chromatography.

[1]Research Institute of Molecular Pathology (IMP), Vienna Biocenter (VBC), Campus-Vienna-Biocenter 1, Vienna 1030, Austria. [2]Institut für Physikalische Chemie, Albert-Ludwigs-Universität Freiburg, Albertstrasse 21, Freiburg 79104, Germany. [3]Department of Neuroscience, The Johns Hopkins University School of Medicine, Baltimore, MD 21205, USA. [4]Institute of Zoology, University of Natural Resources and Life Sciences (BOKU), Vienna, Austria. [5]Department of Organismic and Evolutionary Biology, Harvard University, 16 Divinity Avenue, Cambridge, MA 02138, USA. [6]Institute of Molecular Biotechnology of the Austrian Academy of Sciences (IMBA), VBC, Dr. Bohr-Gasse 3, Vienna 1030, Austria. [7]Monoclonal Antibody Facility, Max Perutz Labs, Medical University of Vienna, Dr. Bohr-Gasse 9, Vienna 1030, Austria. [8]Max Planck Research Group Neurobiology of Magnetoreception, Center of Advanced European Studies and Research (CAESAR), Ludwig-Erhard-Allee 2, Bonn 53175, Germany. [9]Department of Anatomy and Neuroscience, University of Melbourne, Parkville, Australia. [10]Division of Neurobiology, Department Biology II, Ludwig-Maximilians-University Munich, Planegg-Martinsried 82152, Germany.
*Corresponding author. Email: keays@imp.ac.at

Circular dichroism spectra confirmed that the proteins were structured (Fig. 1A). UV-vis absorption spectroscopy revealed that neither clCRY1a nor clCRY2a binds FAD, whereas in the case of clCRY4, we observe maximum absorption at 375 and 450 nm, consistent with the presence of oxidized FAD^{ox} (Fig. 1B). In addition, we observed a broad absorbance peak between 575 and 625 nm that is characteristic of the semiquinone radical ($FADH^{\bullet}$). To determine the rate at which clCRY4 is reduced from FAD^{ox} to $FADH^{\bullet}$ and lastly to the fully reduced $FADH^{-}$ (380 nm), we exposed clCRY4 to blue light (455 nm) and measured spectra at defined intervals. These experiments were performed under three experimental conditions: (i) with oxygen, (ii) without oxygen, and (iii) without oxygen with the electron donor dithiothreitol (DTT) (Fig. 1, C to E). Photochemical reduction proceeded in a stepwise manner; however, complete reduction to the $FADH^{-}$ state was only possible under anaerobic conditions. In anaerobic conditions ($-O_2$ and DTT), sustained exposure of clCRY4 to blue light resulted in a loss of absorption at longer wavelengths (575 and 455 nm), with a single peak remaining at 380 nm, consistent with $FADH^{-}$ (Fig. 1, D and E). A kinetic analysis comparing the rate constants to those obtained for clCRY4 with *Drosophila* cryptochrome (dmCRY) showed that clCRY4 undergoes a rapid and efficient generation of the neutral $FADH^{\bullet}$ state even in the absence of oxygen and electron donors (fig. S1, A to F, and table S1). Next, we asked whether the presence of blue light alters the structure of clCRY4 by undertaking a proteolytic digest. We incubated the native clCRY4 protein with trypsin in the presence and absence of blue light and analyzed the products by denaturing gel electrophoresis. In the absence of light, we found that trypsin

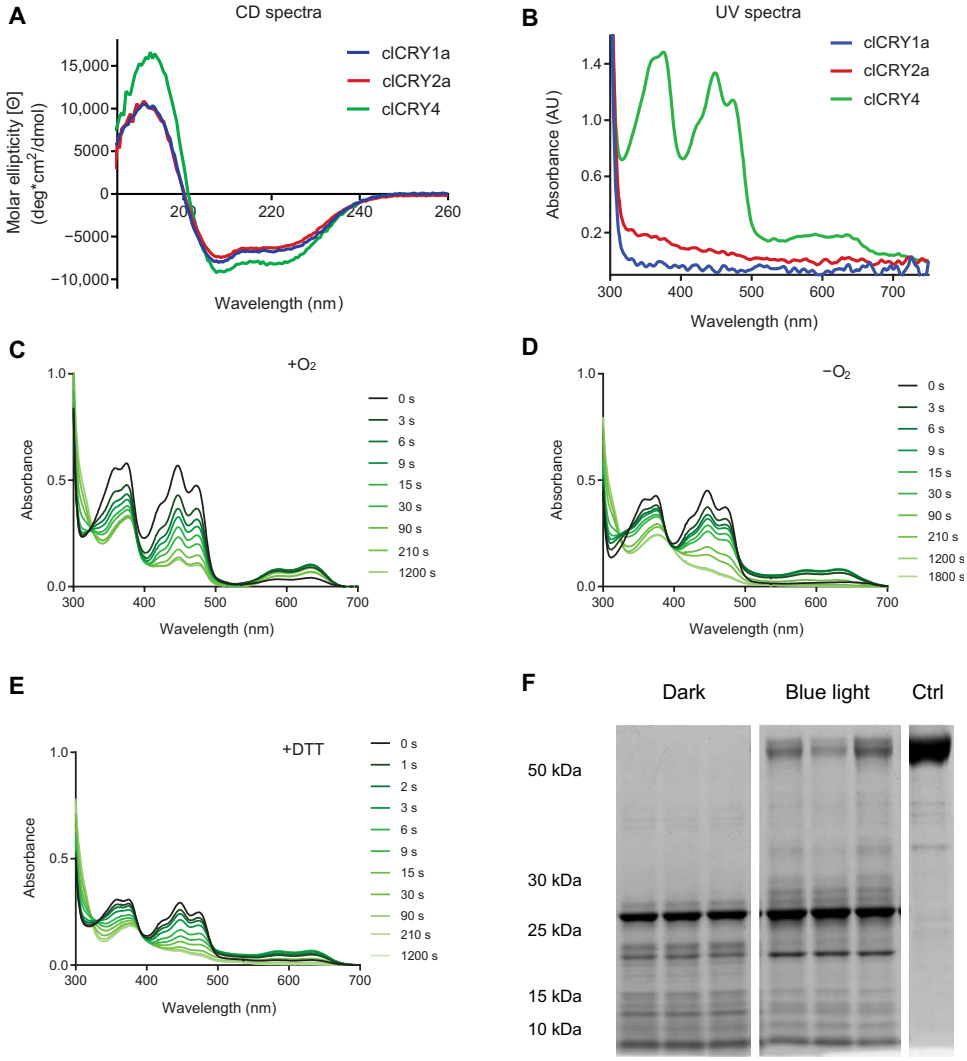

Fig. 1. Photochemical characterization of clCRY4. (**A**) Circular dichroism (CD) spectra showing that the clCRY1a (blue), clCRY2a (red), and clCRY4 (green) proteins are folded correctly. (**B**) UV-vis spectra of clCRY1a, clCRY2a, and clCRY4. We observe no absorbance of clCRY1a and clCRY2a in the visible wavelength range demonstrating that these proteins do not bind FAD. Peaks at ~375 and ~ 450 nm are observed for clCRY4 consistent with the presence of oxidized FAD^{ox}. An additional broad absorbance peak between 575 and 625 nm is characteristic of the presence of a semiquinone radical ($FADH^{\bullet}$). AU, arbitrary units. (**C** to **E**) Photoreduction spectra of clCRY4 following illumination using a 455-nm light source at defined time intervals in the presence of oxygen (C), in the absence of oxygen (D), and with the reducing agent DTT without oxygen (E). Photochemical reduction proceeded in a stepwise manner; however, reduction to the $FADH^{-}$ state (380 nm) was only possible under anaerobic conditions. (**F**) Denaturing gel stained with Coomassie blue following 90-min trypsin digest of native clCRY4. In the dark, we observe a near-complete digest of clCRY4, whereas digestion in the presence of blue light (450 nm) is less efficient, resulting in large bands between 28 and 30 kDa. The control sample was not incubated with trypsin.

resulted in a near-complete digest of the 55-kDa protein, whereas equimolar amounts in blue light were resistant to digest, resulting in the presence of additional bands between 28 and 30 kDa (Fig. 1F). Together, these data confirm that clCRY4 binds FAD, is photoreduced efficiently, and undergoes light-induced conformational changes.

Radical pair formation in pigeon clCRY4

A prerequisite for clCRY4 to function as a quantal-based magnetoreceptor is the capacity to form radical pairs, where the spin correlation of the electrons persists for more than 1 μs (*18*). To ascertain whether this occurs, we undertook transient electron paramagnetic resonance (trEPR) and out-of-phase electron spin echo envelope modulation (OOP-ESEEM) studies on full-length purified clCRY4. These methods enable the identification of the aromatic amino acid involved (either a tryptophan or tyrosine), and provide information on the spin state and distance of the radicals. For trEPR analysis, fully oxidized (FAD^{ox}) clCRY4 was exposed to pulsed laser excitation, and spectra were recorded within a time window of 20 μs at 270 K. The resultant spectra are characterized by an emissive and absorptive peak pattern that has its intensity maximum at ~1 μs after laser excitation, with a single hyperfine pattern that splits at 344.4 mT (Fig. 2A and fig. S2A). Critically, monoexponential fitting showed that the lifetime of the spin-polarized state is 10.06 ± 0.06 μs, enabling modification of the single/triplet yield by external magnetic stimuli (Fig. 2B). Next, we asked which residue within the cryptochrome molecule serves as the final electron donor: TrpA (W395), TrpB (W372), TrpC (W318), TrpD (W369), or Tyr^{319} (Y319). To address this, we undertook simulations of the trEPR spectra using an established spectral simulation protocol (*19*), exploiting published data with respect to the **g** tensors, hfcs, and dipolar (*D*) spin-spin couplings (*20*, *21*) (tables S2 and S3). The spectrum obtained was inconsistent with radical formation with Y319, whereas radical pairs between FAD and TrpC or TrpD could, in principle, reproduce the experimental data (Fig. 2A and fig. S2B). To distinguish between these two possibilities, we undertook an OOP-ESEEM experiment to directly measure the strength of the exchange and dipolar interactions in the radical pair states of clCRY4. Strong echo intensity modulations were observed (Fig. 2C), which were converted into a frequency spectrum, resulting in a Pake-like pattern with turning points at ($\nu_\perp$, $\nu_\parallel$) from which dipolar frequencies and the exchange coupling can be determined (fig. S2C and Table 1). This yielded electron-electron interaction parameters of −8.2 and +0.03 MHz for *D* and J_{ex}, respectively, from which a distance of 2.12 nm can be calculated (*22*). This distance closely mirrors that for FAD-TrpD (2.09 nm) by crystallography (*20*) and permits exclusion of the involvement of a [FAD···TrpC] radical pair (1.75 nm) (Table 1) in wild-type clCRY4. To investigate this further, we generated a TrpD mutant, mutating the tryptophan residue to phenylalanine (W369F), which has a similar aromatic structure but abolishes electron transfer. Previous studies in *D. melanogaster* have shown that this mutation results in TrpC being the final electron donor and the formation of light-induced radical pairs that have a shorter lifetime (*19*). We confirmed that the W369F mutant is structured by performing circular dichroism analysis (fig. S2D), followed by UV-vis spectroscopy that showed that the W369F mutant has an absorption spectrum consistent with the presence of oxidized FAD^{ox} (fig. S2E). trEPR analysis revealed a spectrum similar to wild-type clCRY4, and monoexponential fitting showed that the lifetime of the spin-polarized state was 4.04 ± 0.03 μs (Fig. 2, D and E, and fig. S2F). In contrast to the spectra of the wild type, we did not observe any hyperfine splitting, indicative of radical pair formation between FAD and a different tryptophan. OOP-ESEEM analysis of the W369F mutant showed strong echo intensity modulations; however, the effective frequency was higher (Fig. 2F and fig. S2G). Spectral simulations yielded values of −14.6 and +0.05 MHz for *D* and J_{ex}, respectively, and a distance of 1.75 nm, which is consistent with radical formation between FAD and TrpC in the case of the

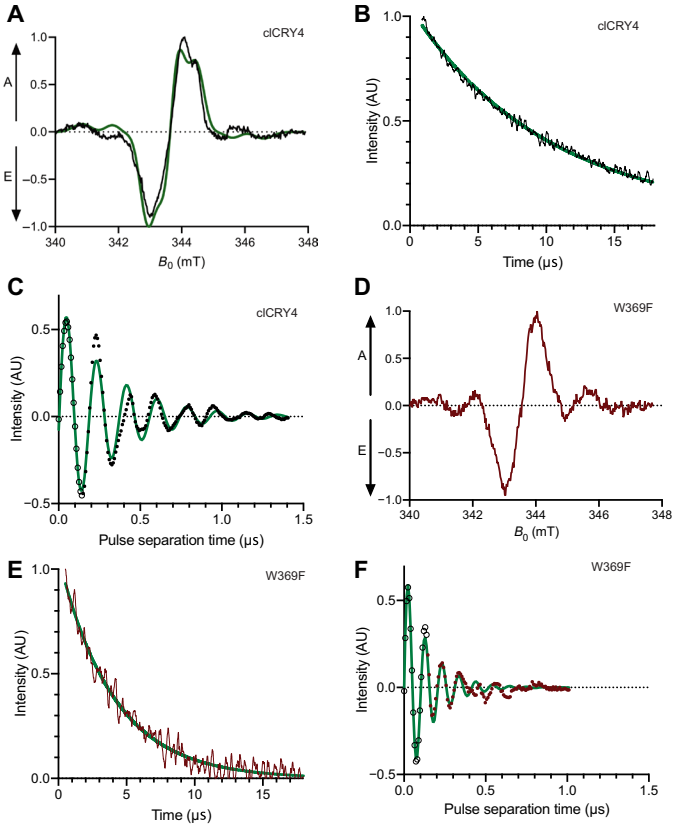

Fig. 2. Radical pair formation in clCRY4. (**A**) trEPR data of clCRY4 recorded at 270 K and a microwave frequency of 9.63 GHz (shown in black). A and E arrows show the enhanced absorptive and emissive signals. The maximum absorptive peak occurs approximately ~1 μs after laser excitation with a single hyperfine pattern that splits at 344.4 mT. The green trace shows the spectral simulation for a [FAD···TrpD] radical pair. (**B**) Graph showing the transient EPR decay curve recorded at 344.2 mT, including a monoexponential fit (shown in green). The lifetime of the spin-polarized radical pair state extracted from the fit results (i.e., the time at which the intensity is decreased by 1/*e* of its maximum value) is 10.06 ± 0.06 μs. (**C**) Q-band OOP-ESEEM of clCRY4 recorded at 80 K. The experimental data are shown with black dots, and open circles show reconstructed data. These data are consistent with a [FAD···TrpD] radical pair in wild-type clCRY4. (**D**) trEPR data of the TrpD mutant (W369F) reveal a similar spectrum to the wild-type protein without hyperfine splitting at 344.4 mT, indicative of radical pair formation with a different tryptophan. (**E**) EPR decay curve of the W369F mutant including a monoexponential fit (shown in green) revealed a reduction in the lifetime of the spin-polarized radical pair state to 4.04 ± 0.03 μs. (**F**) OOP-ESEEM spectra of the W369F mutant that exhibits a higher frequency in comparison to the wild-type protein indicative of an increasing strength of spin–spin coupling and a shorter distance between the two radical pair partners. In the case of the W369F mutation, this distance (1.75 nm) is consistent with a [FAD···TrpC] radical pair. Experimental data are shown with red dots, and open circles show reconstructed data. Green traces in (C) and (F) show spectral simulations, fitted to the experimental data.

Table 1. Summary of known and simulated radical pair parameters for clCRY4. Known distances were extracted from the crystal structure of clCRY4 (*33*), and *D* values were calculated based on the point-dipole approximation. Spectra simulations based on OOP-ESEEM data for wild-type (WT) clCRY4 are consistent with the formation of [FAD···TrpD] radical pairs, whereas in the case of the W369F (TrpD) mutant, the distance mirrors that for a [FAD···TrpC] radical pair.

				Spectral simulations		
Radical pair	**Known distance**	**Calculated *D* (MHz)**	**Sample**	***D* (MHz)**	**J_{ex} (MHz)**	**Distance (nm)**
[FAD···TrpD]	2.09 nm	−8.5	clCRY4 WT	−8.2 ± 0.2	+0.03 ± 0.05	2.12 ± 0.02
[FAD···TrpC]	1.75 nm	−14.5	clCRY4 W369F	−14.6 ± 0.2	+0.05 ± 0.05	1.75 ± 0.01

W369F mutant (Table 1). Together, these data show that wild-type clCRY4 forms long-lived spin-correlated radical pairs between FAD and TrpD, enabling it to function as a light-based quantal magnetoreceptor.

Expression analysis of *clCRY4* mRNA

Next, we examined the expression of *clCRY4* in 10 different tissues by undertaking quantitative polymerase chain reaction (qPCR) ($n = 3$). This revealed that *clCRY4*, like *clCRY1a*, *clCRY1b*, *clCRY2a*, and *clCRY2b*, is broadly expressed throughout the pigeon (fig. S3, A to E). Focusing on the retina, we asked whether clCRY4 is under circadian regulation. Sampling transcript levels at eight different time points at 3-hour intervals ($n = 3$ birds) showed that its expression levels vary little over the course of the day (fig. S3J). This is in marked contrast to *clCRY1a*, *clCRY1b*, *clCRY2a*, and *clCRY2b* that exhibit oscillatory expression patterns (fig. S3, F to I). Next, we investigated the spatial expression of *clCRY4* mRNA by performing laser microdissection of the retina ($n = 3$). We dissected out the ganglion cell layer (GCL), the inner inner nuclear layer (iINL), the outer inner nuclear layer (oINL), and the outer nuclear layer (ONL) (fig. S4, A to D; $n = 3$ birds). We confirmed the validity of our laser dissection by testing known qPCR markers for ganglion cells (*clTHY1*), bipolar cells (*clVSX2*), and photoreceptors (*clRHO*) (fig. S4, F to H, and table S4). qPCR showed that *clCRY4* mRNA is present within all retinal layers and is expressed at highest levels in the ONL and oINL (where the soma of horizontal cells reside) (fig. S4E). Together, these data show that the *clCRY4* transcript is broadly expressed at stable levels within the retina.

Localization of the clCRY4 protein in the retina

To further interrogate the localization of clCRY4, we generated two monoclonal antibodies (2B5 and 7C11) using a C-terminal antigen (H405-E525), which we carefully validated (fig. S5, A to E). We then undertook histological analysis of retinal sections, initially using a permanent staining protocol (Fig. 3, A and E). Consistent with our laser microdissection results, we observed broad staining in all layers of the retina for both the 2B5 and 7C11 clCRY4 antibodies. This staining was abolished when the antibodies were preabsorbed with the antigen (fig. S6, A to C). We observed a notable enrichment of clCRY4 signal in the ganglion cells, the outer limiting membrane, as well as distinct horizontal stripes staggered at regular intervals in the outer plexiform layer (OPL) when staining with both the 2B5 and 7C11 antibodies (Fig. 3, A and E). High-resolution confocal analysis using fluorescent secondary antibodies revealed that the horizontal stripes in the OPL had a concave morphology and were arranged in two distinct layers, which was most pronounced in the innermost layer (Fig. 3, B to D and F to H). This staining pattern resembles that reported for GluR1, GluR2/3, and GluR4, which labels glutamatergic synapses between cones and horizontal cells known as pedicles (*23*). To investigate this further, we performed double staining using our clCRY4 antibodies and sera that target calretinin, which labels brush-shaped H1 horizontal cells in multiple species, with distinct dome-shaped staining at cone pedicles (*24*). We observed a thin line of clCRY4 staining directly below calretinin-positive synapses, consistent with a postsynaptic localization (Fig. 3, I to N). We conclude that clCRY4 is broadly expressed within the pigeon retina but is enriched within the OPL at synapses between photoreceptors and horizontal cells.

The clCRY4 interactome

To further explore the function of clCRY4, we set out to define its interaction partners. To do so, we performed coimmunoprecipitation experiments using both our cryptochrome antibodies and a green fluorescent protein (GFP) monoclonal to control for nonspecific binding. Retinal, cerebellar, and liver lysates were prepared from tissues collected at midday, mechanically lysed, and exposed to magnetic Dynabeads conjugated with the 2B5 and 7C11 antibodies. The attached proteins were eluted and trypsinated, and their sequences were determined by mass spectrometry. We exploited the available pigeon genome to annotate each protein (*25*). Using the 2B5 antibody, we identified 92 putative interactors in the retina, 70 in the cerebellum, and 49 in the liver (Fig. 4A and table S4). Using the 7C11 antibody, we identified 95 putative interactors in the retina, 64 in the cerebellum, and 42 in the liver (Fig. 4B and table S4). The most abundant protein immunoprecipitated in our retina samples was clCRY4, which was not present in the GFP control pulldown, demonstrating the effectiveness of our methodological approach and further validating our antibodies. We reasoned that if clCRY4 plays a role in magnetosensation, then it likely relies on interaction partners and a signaling network that is present in the retina but absent in the cerebellum and liver. Comparative analysis showed that eight proteins were precipitated by both the 2B5 and 7C11 antibodies that were retinal specific. They are as follows: a TIMELESS homolog, GRIP1, GRIP2, WAPL, NGLY1, CASK, FRG1, and PIP4K2B. A gene ontology analysis on the molecular function of these eight proteins revealed a significant enrichment for receptor signaling complex adaptor activity and signaling adaptor activity (Fig. 4C). GRIP1 and GRIP2 are PDZ domain–containing scaffolding proteins that are associated with the targeting and anchoring of glutamate receptors to the postsynaptic membrane (*26*, *27*).

To confirm that TIMELESS, GRIP1, GRIP2, WAPL, NGLY1, CASK, FRG1, or PIP4K2B proteins interact with clCRY4, we performed a reciprocal coimmunoprecipitation. The FLAG-tagged interactors were coexpressed in Neuro2A cells with MYC-tagged clCRY4. We then immunoprecipitated these interactors using anti-FLAG beads and performed denaturing gel electrophoresis followed

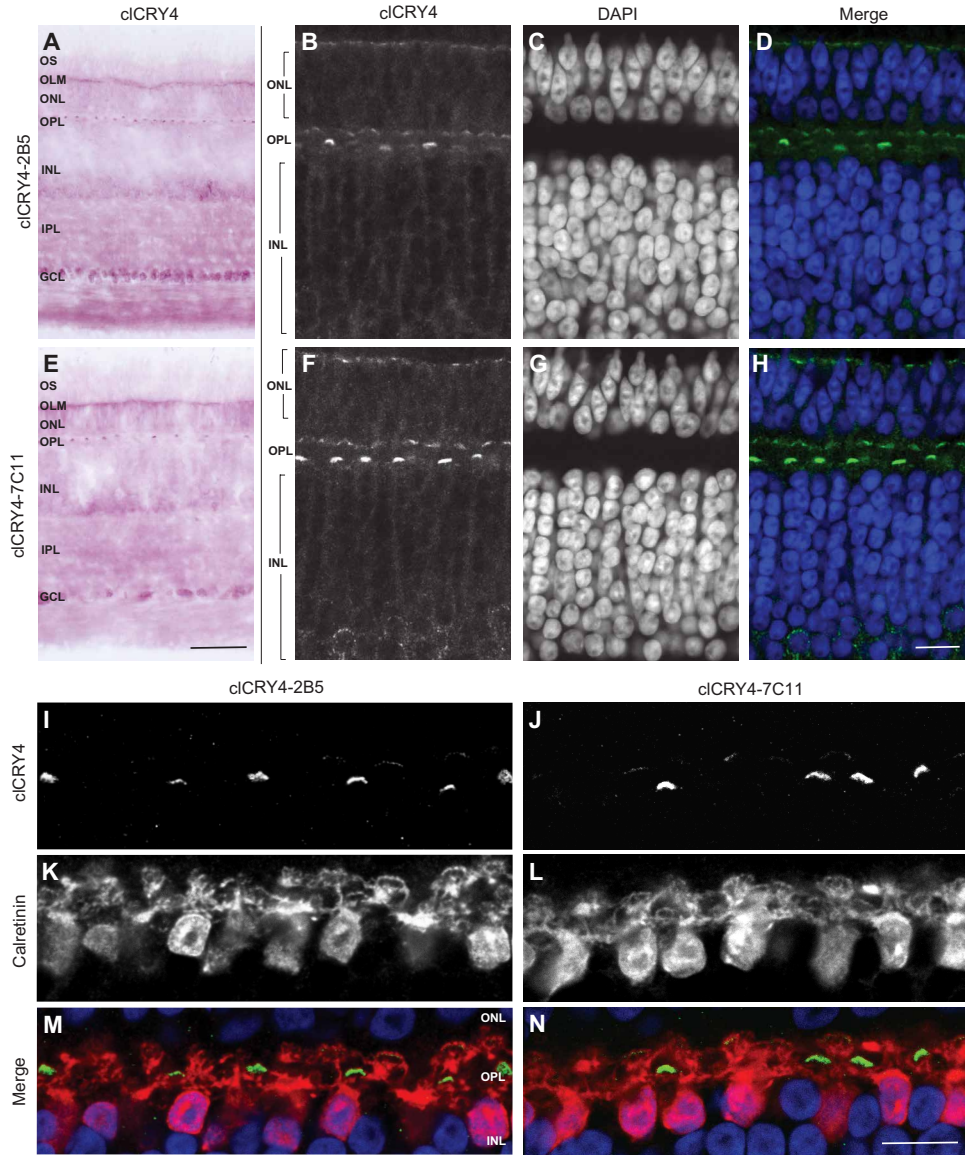

Fig. 3. Localization of the clCRY4 protein in the retina. (**A** to **H**) Immunohistochemistry using the clCRY4-7C11 and clCRY4-2B5 antibodies on the adult pigeon retina harvested at midday ($n = 10$). (A and E) Overview of the retina using a permanent staining protocol reveals that clCRY4 is broadly expressed throughout the retina and is enriched in ganglion cells (GCL) and the OPL and in the outer limiting membrane (OLM). (B to D and F to H) Confocal images using fluorescent secondary antibodies highlighting the inner nuclear layer (INL), OPL, and the outer nuclear layer (ONL). clCRY4-enriched crescents in the OPL are arranged in two distinct layers with the most pronounced in the innermost layer. (B and F) Images showing clCRY4 staining only, (C and G) 4′,6-diamidino-2-phenylindole (DAPI) staining, and (D and H) merged images of clCRY4 and DAPI. clCRY4 is largely absent from DAPI-positive nuclei. (**I** to **N**) High-resolution confocal images focused on the OPL using sera against calretinin, which labels horizontal cells. The clCRY4 staining appears directly beneath a dome of calretinin staining, consistent with a postsynaptic localization within horizontal cells. (I and J) Images showing clCRY4 staining only, (K and L) calretinin staining, and (M and N) merged images of clCRY4 and calretinin. OS indicates the outer segments of photoreceptors and IPL denotes the inner plexiform layer. Scale bars, 50 μm (E) and 10 μm (H and N).

by immunoblotting. Staining with anti-FLAG antibody confirmed expression of our target interactors (fig. S6E), and MYC immunoblotting demonstrated direct clCRY4 interaction with all eight putative interactors that was most pronounced for PIP4K2B and GRIP2 (Fig. 4D). We focused on the GRIP proteins as their expression is enriched in the plexiform layers of the retina (*28*). We predicted that the GRIP proteins would colocalize with clCRY4 in the pigeon retina. We obtained an N-terminal polyclonal GRIP2 antibody and confirmed by Western blot analysis that it binds to the pigeon protein in retinal lysates (fig. S6D). Using this antibody, we performed immunohistochemistry with our 2B5 and 7C11 CRY4 antibodies along with GRIP2 (Fig. 4, E to P). Consistent with reported studies, we observed punctate staining in the OPL for GRIP2 (*28*). High-resolution confocal microscopy showed clear colocalization with cryptochrome, GRIP2 often mirroring the crescent shape discs of clCRY4 staining (Fig. 4, K to P). Last, we asked whether the clCRY4-GRIP1/2 interaction that we observe might be the product of cross-reactivity of our clCRY antibodies. To address this, we

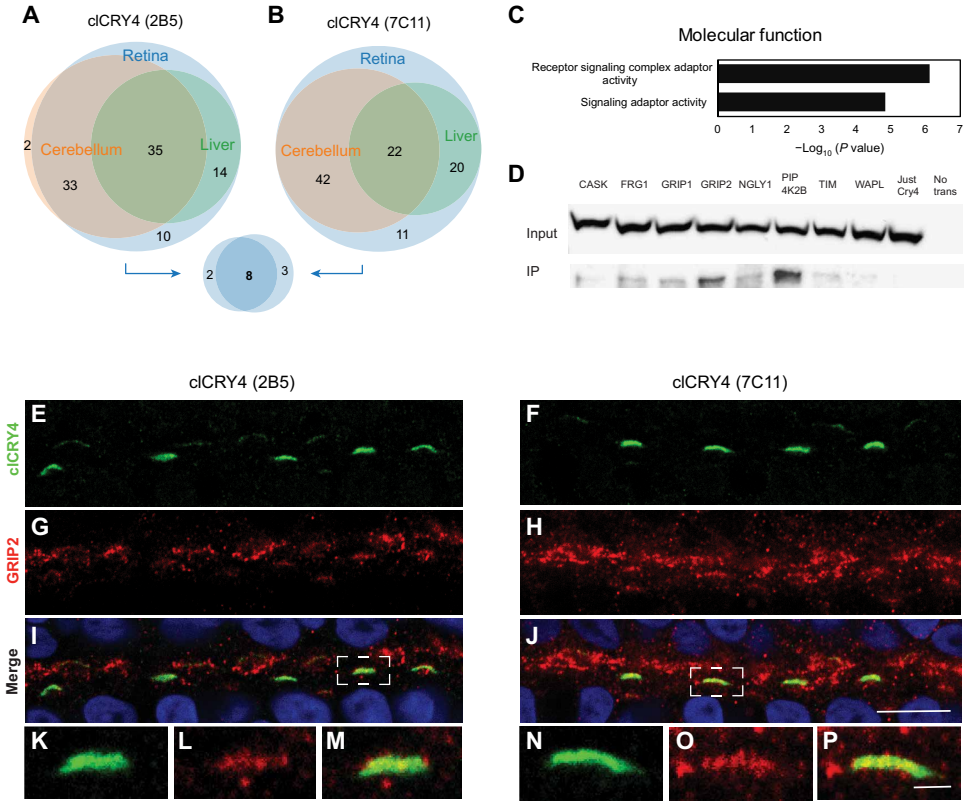

Fig. 4. clCRY4 interaction partners. (**A** and **B**) Venn diagram showing clCRY4 putative interactors immunoprecipitated with the 2B5 and 7C11 antibodies from the retina, the cerebellum, and the liver. (A) With the 2B5 antibody, we identified 92 putative interactors in the retina, 70 in the cerebellum, and 49 in the liver. (B) With the 7C11 antibody, we identified 95 putative interactors in the retina, 64 in the cerebellum, and 42 in the liver. (**C**) A gene ontology analysis of the shared CRY4 2B5/7C11 retinal hits using PANTHER revealed an enrichment of molecules associated with receptor signaling activity. (**D**) Validation of putative clCRY4 interactors by reciprocal coimmunoprecipitation in Neuro2A cells. FLAG-tagged putative interactors were coexpressed with MYC-tagged clCRY4, before immunoprecipitation with anti-FLAG beads. Blots show anti-MYC staining of SDS–polyacrylamide gel electrophoresis (SDS-PAGE) gels for cell lysates (input) and immunoprecipitation eluates (IP). No signal is visible in untransfected cells or those cells expressing MYC-clCRY4 alone. Notable clCRY4 interaction is observed with GRIP2 and PIP4K2B. (**E** to **P**) Immunostaining of the OPL of the retina using the clCRY4 2B5 and 7C11 antibodies (green, E and F) with an antibody targeting GRIP2 (red, G and H). High-resolution confocal analysis shows colocalization with GRIP2 mirroring the crescent shape of clCRY4 staining (K to P). Scale bars, 10 μm (J) and 2 μm (P).

overexpressed GRIP1-FLAG, GRIP2-FLAG, and clCRY4 in Neuro2A cells and analyzed the lysates by denaturing gel electrophoresis probing with an anti-FLAG antibody and our clCRY4 7C11 and 2B5 antibodies. This confirmed that our clCRY4 antibodies bind with strong affinity to clCRY4 and showed that they do not cross-react with either GRIP1 or GRIP2 (fig. S6F). Together, these data show that clCRY4 interacts with proteins that modulate receptor signaling, including GRIP1/2.

DISCUSSION

In this study, we have explored whether clCRY4 has the molecular and biophysical attributes to function as a magnetosensor. Consistent with a number of recent studies, we have shown that clCRY4 binds FAD and undergoes a rapid and efficient generation of the semiquinone radical state ($FADH^{\bullet}$) when exposed to blue light (*20*, *29*). We have further demonstrated that, in anaerobic conditions, clCRY4 (unlike *Drosophila* cryptochrome) can be fully reduced to $FADH^{-}$. This raises the prospect that clCRY4 relies on two different signaling states ($FADH^{\bullet}$ and $FADH^{-}$), depending on the oxygen availability. By exploiting trEPR and OOP-ESEEM, we have shown that clCRY4 forms long-lived radical pairs, with a spin-polarized state that exceeds 10 μs, and that TrpD (W369) is the final electron donor. The ability to form long-lived coupled radical pairs is critical for the RPM as it enables external magnetic fields to influence the ratio of triplet-singlet spin states, altering the structural properties of the sensor, which we expect would occur within milliseconds (*30*). While the majority of our spectroscopic data are consistent with that of Zoltowski and colleagues, our conclusions differ with respect to the residue that forms the spin-polarized radical. They have argued that clCRY4 forms a radical between FAD and Tyr^{319} (*20*); however, our trEPR spectra are inconsistent with such a radical. Moreover, the 2.12-nm distance of the two radicals obtained from OOP-ESSEM is far shorter than the ~2.4-nm distance of a hypothetical [FAD···Tyr] radical pair. Last, it should be noted that the trEPR spectrum of clCRY4 that we report in this paper differs from *Drosophila* cryptochrome although the TrpD residues are at identical positions/orientations according to the respective crystal structures (*31*–*33*). We attribute this difference to an increased flexibility of TrpD, which is reflected by the *B* factors that describe the conformational freedom of the residue (table S3). We expect that this flexibility would also have a significant impact on the properties of the radical pair and how it is influenced by external magnetic fields.

To define the expression of clCRY4, we have exploited qPCR, laser microdissection, and immunohistochemistry. We report that *clCRY4* mRNA is broadly expressed throughout the pigeon, that it is stably expressed in the retina, that it is found in all retinal layers, and that the protein is enriched at synapses in the OPL. Our finding that clCRY4 exhibits stable expression in the retina, unlike the oscillatory nature of clCRY1a/b and clCRY2a/b, is consistent with a number of previous studies including that of Muheim and colleagues who studied CRY4 expression in zebrafinches (*34*, *35*). The broad expression pattern of clCRY4 that we report here reflects the findings of Okano and colleagues who reported that, in chickens, CRY4 is expressed in all tissues at low levels and that the mRNA is present in all retinal cell types (*36*, *37*). In contrast to our results, it has been reported that the CRY4 protein is specifically expressed in the outer segments of double cones and long-wavelength single cones in European robins and chickens (*35*). While this may be due to species-specific or seasonal variation in CRY4 expression, these differences might also be attributed to methodological issues such as the utilization of a tertiary enhancing antibody by Günther and colleagues. The enrichment of clCRY4 in two distinct layers in the OPL is intriguing. This pattern of staining is reminiscent of that reported for glutamate receptors and PSD-95 (postsynaptic density protein 95) at cone pedicles (*23*). Cone pedicles are 5 to 8 μm wide, consisting of a cone with ribbon synapses between two horizontal cells and a bipolar cell (*38*). In pigeons, pedicles are known to be stratified with red or green sensitive cones terminating in the intermediate OPL, whereas blue sensitive cones have synaptic endings in the innermost stratum (*38*). Intriguingly, our clCRY4 staining is markedly stronger in the innermost region of the OPL, raising the prospect that it is preferentially associated with blue cone pedicles. An advantageous attribute for a quantal-based magnetoreceptor is some ordering of the receptive molecules; otherwise, the directional information of randomly orientated molecules averages to zero (*3*). If clCRY4 molecules are tethered to the postsynaptic membrane, as our data suggest, then this would provide the necessary anisotropy for the molecule to function as a magnetoreceptor.

To gain insight into the molecular function of clCRY4 and the signaling pathway in which it operates, we have used mass spectroscopy to identify interactors in the retina, cerebellum, and liver. This study efficiently immunoprecipitated clCRY4, pulled down known interactors (e.g., TIM, PPP2R5D), and identified approximately 100 putative interactors. These include proteins involved in a broad range of cellular processes including cytoskeletal biology (e.g., MAP1B and KIF2C), RNA processing (RPS6 and RPL8), regulation of the cell cycle (e.g., PPP2R5C, PPP2R5D, and WAPL), and signaling adaptor activity (SYN, NECAB2, and GRIP2). These data strongly suggest that clCRY4 is not functionally monogamous. To assess the feasibility of clCRY4 as a magnetoreceptive molecule, we have focused on those proteins that interact with it in the retina, but not the cerebellum and liver. This analysis highlighted molecules associated with glutamatergic receptor signaling. Both our clCRY4 antibodies pulled down GRIP1 and GRIP2 from retinal lysates, we confirmed that GRIP1/2 interact with clCRY4 by reciprocal coimmunoprecipitation in a cell culture system, and we have shown that GRIP2 and clCRY4 colocalize at horizontal cell synapses within the retina. The GRIP proteins have been implicated in the trafficking of glutamate receptors (e.g., GluR 2/3) to the synapse and the coupling of these receptors to intracellular machinery. It has been shown that deletion of GRIP1/2 alters the phosphorylation status of Glu2A and perturbs synaptic plasticity in the cerebellum of mice (*39*–*41*). Accordingly, our work raises the intriguing possibility that magnetic stimuli in the presence of light influence the efficiency of glutamatergic synaptic transmission in the OPL of the retina through a clCRY4-GRIP1/2 signaling pathway. An analogous mechanism exists in *Drosophila*, whereby blue light directly influences neuronal depolarization via a redox-dependent potassium channel (Kvβ) that is dependent on the integrity of the tryptophan tetrad in CRY molecules (*42*). In *Drosophila*, it has been further demonstrated that CRY also functions as a UV sensor (*43*). An alternative explanation for our results is that clCRY4 augments UV sensitivity (which is primarily mediated by the short-wave opsin SWS1) and that the formation of long-lived radicals is merely coincidental to that function (*44*). Given the absence of clCRY4 homologs in mammals, it is conceivable that other light-sensitive molecules exist that may function as magnetic sensors. It is also important to emphasize that our results do not exclude the presence of complementary light-independent mechanisms that rely on magnetite or alternatively electromagnetic induction (*45*). Despite these caveats, our data support a model whereby clCRY4 acts as a UV-blue photoreceptor and/or a light-dependent magnetosensor by modulating glutamatergic synapses between horizontal cells and cones (Fig. 5).

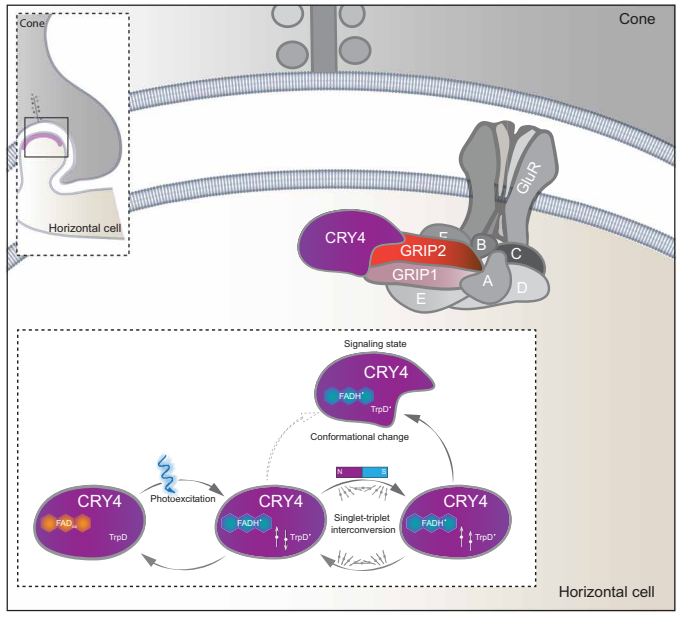

Fig. 5. Model illustrating how clCRY4 could act as a UV/blue photoreceptor and/or magnetoreceptor. clCRY4 (shown in purple) is enriched postsynaptically at cone pedicles and interacts with a complex that includes GRIP1/2 and glutamate receptors (GluR). Upon excitation with light in the blue/UV spectrum, the oxidized flavin (FAD^{ox}) embedded within clCRY4 abstracts an electron from TrpA, reducing it to $FADH^{\bullet}$ and concomitantly forms a short-lived tryptophan radical. This initiates a stepwise electron transfer from TrpB, then from TrpC, before the terminal surface-exposed TrpD radical is formed. This generates a long-lived spin-correlated radical pair between [FAD···TrpD] (shown in bottom inset). The spin state (i.e., singlet or triplet) of this coupled radical pair is influenced by the external magnetic environment, which affects the efficiency and/or degree of light-induced clCRY4 conformation change. This structural change affects clCRY4 interaction with GRIP1/2 (and/or other postsynaptic partners), thereby altering the properties of glutamatergic synapses in the OPL of the retina.

MATERIALS AND METHODS

Cloning of pigeon cryptochromes

To clone the pigeon cryptochromes, retinal complementary DNA (cDNA) libraries were used. PCR primers for the pigeon *clCRY* transcripts were designed on the basis of the annotated pigeon sequences for *clCRY1a*, *clCRY2a*, and *clCRY4* using the Primer3Plus software tool (www.bioinformatics.nl/cgi-bin/primer3plus/primer3plus.cgi). Several primer sets (amplicons sized between 500 and 1500 nt) were designed for each cryptochrome to cover the complete coding region of each transcript. To identify the putative *clCRY1b* splice isoform, as well as the 5′ and 3′ untranslated regions of each transcript, an adaptor-ligated retinal cDNA library for amplification of cDNA ends was generated according to the manufacturer's instructions (Clontech, 634923). For all PCR reactions, a proofreading high-fidelity DNA polymerase (Thermo Fisher Scientific, F-549S) spiked with a non-proofreading polymerase (Qiagen, 203205) was used to generate PCR products with 3′ A-overhangs suitable for TA cloning. The PCR products were cloned into a TOPO pCR 2.1 vector (Thermo Fisher Scientific, K4520-01) and analyzed by Sanger sequencing.

Protein expression

The coding sequence of clCRY1a, clCRY2a, and clCRY4 were cloned into pFLN2 to generate bacmid viruses using the Bac-to-Bac baculovirus expression. Sf9 Insect cells were transfected with the baculovirus and centrifuged at 4000 rpm for 15 min. Pellets were resuspended in 50 ml of lysis buffer [50 mM Hepes, 400 mM NaCl, 10% glycerol, 0.5% Triton X-100, and 0.5 mM TCEP (Tris(2-carboxyethyl) phosphine) (pH 8.0)] with 5 μl of benzonuclease and a tablet of EDTA-free protease inhibitor (Sigma-Aldrich, 11836170001). Cells were then lysed via douncing, and the lysate was centrifuged at 18,000 rpm for 1 hour. His-tagged cryptochromes were purified by Ni–nitrilotriacetic acid affinity chromatography (GE Healthcare, 17524802) with a running buffer [50 mM Hepes, 150 mM NaCl, 20 mM imidazole, 10% glycerol, and 2 mM TCEP (pH 8.0)]. Column-bound proteins were eluted with an imidazole gradient in an elution buffer [50 mM Hepes, 150 mM NaCl, 300 mM imidazole, 10% glycerol, and 2 mM TCEP (pH 8.0)]. Eluted peaks were collected and concentrated [Pierce Protein Concentrator, 10K molecular weight cutoff (MWCO)] to a maximum volume of 10 ml before being loaded on a size exclusion column (GE Healthcare, HiLoad 26/600 Superdex 200, 28-9893-36). Size exclusion was performed with a running buffer [50 mM Hepes, 150 mM NaCl, 2 mM TCEP, and 10% glycerol (pH 8.0)], and collected fractions were analyzed on SDS–polyacrylamide gel electrophoresis (SAS-PAGE) gels (NativePAGE 3 to 12% Bis-Tris, Invitrogen). Cryptochromes were then concentrated using a commercial column (Pierce Protein Concentrator, 10K MWCO).

UV-vis absorption and circular dichroism measurements

clCRY1a, clCRY1b, and clCRY4 samples were measured at a concentration of 2 mg/ml in 50 mM Hepes, 150 mM NaCl, 2 mM TCEP-HCl, and 10% glycerol (pH 8.0). Spectra were collected with a spectrophotometer (DeNovix DS-11, FX+) with a 10-mm pathway. Absorption spectra were collected from 220 to 750 nm. To verify that our purification protocol resulted in folded and stable protein, we prepared samples of the different constructs at 0.2 mg/ml and checked for secondary structural elements. Samples were measured at a concentration of 0.2 mg/ml using a Chirascan Plus CD Spectrometer in 20 mM Na_2HPO_4 and 150 mM NaF. Spectra were collected from 280 to 190 nm. For our steady-state photoreduction experiments, measurements were taken on a UV-vis spectrometer (Shimadzu, UV-2450). Photoreduction kinetics were recorded either under aerobic conditions, under anaerobic conditions, or under anaerobic conditions in the presence of 2 mM DTT. To degas the sample, argon gas was bubbled through the sample solution for 30 min. Before any measurement, the protein solution was left 5 min in the dark to ensure the 100% dark state before spectra were recorded. Spectra were measured at defined times after illumination using a light-emitting diode emitting at 455 nm (65.8 mW/cm^2; Thorlabs, M455L4). The photoreduction kinetics was analyzed as described previously (*46*).

Limited proteolysis

Limited proteolysis was performed using sequencing-grade modified trypsin (Promega, V5113) with a 1:50 trypsin-to-protein (w/w) ratio in size exclusion buffer [50 mM Hepes, 150 mM NaCl, 10% glycerol, and 2 mM TCEP (pH 8.0)]. clCRY4 protein aliquots were prepared (40 μl at 0.6 mg/ml), before the addition of 9.6 μl of trypsin (0.05 mg/ml). Samples were incubated in either the dark or illuminated with blue light (462 nm) at a total irradiance of 560.817 $\mu W/cm^2$ for 90 min. For nonirradiated samples, light safe tubes were used (Sigma-Aldrich, Z688312). The reaction was stopped using an equal amount of 2× SDS loading dye (Thermo Fisher Scientific, B0007) and heated for 5 min at 95°C. Samples were resolved on a 4 to 12% Bis-Tris precast polyacrylamide gel (Thermo Fisher Scientific, NW04125BOX) in 1× Mops buffer (Thermo Fisher Scientific, B000102). The gel was stained with Coomassie blue.

Transient EPR spectroscopy

clCRY4 samples were prepared in a buffer containing 50 mM Hepes (pH 8.0), 150 mM NaCl, and 50% (v/v) glycerol. Sample concentrations were determined using UV-vis spectroscopy (Shimadzu, UV-2450) on the basis of the absorption maximum at 447 nm and an extinction coefficient of 11,300 liters mol^{-1} cm^{-1}. $K_3[Fe(CN)_6]$ (10 eq) was added, and samples were adjusted to a final concentration of ~1 mM for clCRY4 wild type. X-band transient EPR (trEPR) spectra of clCRY4 samples were recorded following pulsed laser excitation, which was performed using an OPO system pumped by a Nd:YAG laser (Ekspla, NT342B-20) at a wavelength of 445 nm and a pulse energy of (1.5 ± 0.1) mJ at a repetition rate of 1 Hz (pulse duration, 4 ns). A custom-built spectrometer was used in combination with a Bruker microwave bridge (Bruker, ER046 MRT). The sample was placed in a synthetic quartz tube with an inner diameter of 1 mm (outer diameter, 1.6 mm) and irradiated in a dielectric resonator (Bruker, ER4118X-MD5). The resonator was immersed into a laboratory-built nitrogen gas-flow cryostat, and data were collected at a temperature of (270.0 ± 0.5) K stabilized by a temperature controller (Oxford Instruments, ITC503). The microwave power was set to 2 mW, and the microwave frequency was controlled by a frequency counter (Keysight Technologies, 5352B). Signal acquisition was performed with a transient recorder (Teledyne LeCroy, 9354A) at a bandwidth of 25 MHz. Distortions of the signal baseline introduced by the laser pulse were corrected by subtracting a signal collected at an off-resonant magnetic field position of 280 mT. Fitting of time-dependent trEPR signals (t) was performed by least-squares fitting using the model function $I(t) = I_{off} + I_0 \cdot \exp(-t/\tau)$, where I_{off} is the data offset, I_0 is the maximum amplitude, and τ is a time constant that defines the strength of the decay. The value of τ is the corresponding time value at which the amplitude is decreased by

1/*e* of its maximum value. Here, τ is defined as the lifetime of the spin-polarized radical pair state.

Spectral simulation of trEPR data

Simulations of trEPR spectra were performed using a self-written Python routine, based on the radical pair model and the FORTRAN program described previously (*19*, *21*). This approach includes the **g** and **A** tensors as well as the electron-electron interactions in the fitting process. The dipolar coupling *D* was calculated on the basis of the point-dipole approximation using $D/\mathrm{mT} = -2.782/(\frac{r}{\mathrm{nm}})^3$. As point of highest spin density, the spin-density weighted average of the density functional theory–calculated electron spin densities was calculated and used for FAD, tryptophan, and tyrosine, respectively. The parameters are summarized in table S2.

Out-of-phase electron spin echo envelope modulation experiments

OOP-ESEEM data were recorded at Q-band frequencies using a commercially available FT-EPR (Fourier transform electron paramagnetic resonance) spectrometer (Bruker Elexsys, E580) equipped with an AMPX10 solid-state amplifier for microwave-pulse amplification. Protein samples were placed into synthetic quartz tubes (Suprasil, Heraeus Quarzglas GmbH & Co. KG) with an inner diameter of 1 mm (outer diameter, 1.6 mm) and irradiated in a dielectric-ring resonator (Bruker EN 5107D2). The resonator was immersed into a helium gas flow cryostat (Oxford Instruments, Oxford CF-935) stabilized to (80.0 ± 0.5) K by a temperature controller (Oxford Instruments, Oxford ITC4). Pulsed laser excitation of the sample was performed using an OPO system pumped by a Nd:YAG laser (Ekspla, NT342B-20) at a wavelength of 445 nm and a pulse energy of (1.0 ± 0.1) mJ at a repetition rate of 20 Hz (pulse duration, 4 ns). The OOP-ESEEM pulse sequence was used with τ_{DAF} = 200 ns (DAF, delay after flash) (*47*). The first and second pulse lengths were 24 and 48 ns, respectively, at a magnetic field of 1202.3 mT (microwave frequency, 33.71 GHz). The time interval between the two microwave pulses (τ) was varied in 8-ns steps where the minimal τ value was limited by the spectrometer death time (about 150 ns). Echo detection was performed by integrating over the echo intensity. Analysis of OOP-ESEEM data was carried out on the basis of published procedures (*22*). In detail, time-domain data were converted into frequency spectra by sine Fourier transformations (fig. S2). A Pake doublet with turning points at ($\nu_\perp$, $\nu_\parallel$) and ($\nu_\perp'$, $\nu_\parallel'$), which are characteristic of spin-correlated radical pairs, was observed. *D* and J_{ex} were obtained from these frequencies by applying the following formulas: $D = \frac{\nu_\perp - \nu_\parallel}{2}$ and $J_{ex} = (2\nu_\perp - \nu_\parallel)/6$. Both echo decays and frequency spectra were analyzed permitting extraction of the exchange couplings. The distance was obtained using the point-dipole approximation. Error margins of *D* and J_{ex} were obtained using the Cramer-Rao lower bounds theorem (*48*). If the least-squares fittings yielded different values of equal quality, then the errors were rounded to higher values.

Real-time qPCR

Adult pigeons were euthanized at defined time points, and their tissues were harvested before snap freezing in liquid nitrogen and storage at −80°C. For the analysis of cryptochrome expression in a broad range of tissues (beak skin, cochlear, heart, kidney, liver, olfactory epithelium, pineal gland, respiratory concha, spleen, and telencephalon), samples were collected at midday (12:00 p.m.). For the temporal analysis of cryptochrome expression in the retina, samples were harvested at 3-hour intervals over the course of 24 hours. For RNA isolation, the tissues were homogenized in a TissueLyser II using 3-mm carbide beads (Qiagen, 69997). Total RNA was extracted using the RNeasy Mini Kit (Qiagen, 74104) according to the manufacturer's protocol. RNA was reverse-transcribed using the QuantiTect reverse transcription kit (Qiagen, 205314) to generate cDNA for real-time qPCR analysis. For qPCR analysis, intron-spanning primers were designed using the Primer3Plus program. Following primer efficiency testing, primer pairs with an efficiency of 90 to 105% were selected for each transcript. To ensure that the primers were specific for each cryptochrome isoform, we undertook the following measures: (i) we conducted BLAST searches against the pigeon genome to limit promiscuous binding of our primers; (ii) we ensured that each primer set was exon spanning to prevent the amplification of genomic DNA; (iii) we confirmed that each PCR product produced a single melt curve when analyzed on the qPCR machine; and (iv) we confirmed the identity of our amplicons by agarose gel electrophoresis and Sanger sequencing. We used the following primers: *clCRY1a_F*, GAGACTCGCATACAGGAGCAA; *clCRY1a_R*, TGTCTCCATGAGCATAGTGTAAGA; *clCRY1b_F*, GCATTTCTGGTTGTGGTAGTACAG; *clCRY1b_R*, ATTTGGAGATCCTCTACAGACAGG; *clCRY2a_F*, GGAAGAGCTGGGCTTTCCTAC; *clCRY2a_R*, TTCTTTCCAAGTGTTTATCCAGCC; *clCRY2b_F*, TGTAAAGTGGACATCCAGGAGAAC; *clCRY2b_R*, ATTTGAAGCCATGCCCAGCTC; *clCRY4_F*, AACATTTACGCTCAGGCCAAGCAC; *clCRY4_R*, GCCGATGCCACCGTGTAGAAGAA; *clHPRT_F*, CTCCTCGAAGTGTGG; *clHPRT_R*, AGTATTCATTGTAATCTAGGG; *clGAPDH_F*, TCAATGGGAAACTTACTGGAATGG; *clGAPDH_R*, TCTTAATGTCATCATACTTGGCTGG; *clTFRC_F*, CATATTATTGGAACTTGCCCGTGT; *clTFRC_R*, CCACAGCTCCATACTCTCCT; *clTHY1_F*, CTACACTGGCAACCAGATAAAGAA; *clTHY1_R*, GTTCTGGATCAAGAGGCTGAAG; *clVSX2_F*, ACAATCTTCACATCCTACCAACTG; *clVSX2_R*, GAACCAAACCTGTATCCTGTCTTC; *clRHO*_F, GTTCTACATCTTCACCAACCAGG; *clRHO_R*, CAGAGAGTTGTGATCATGCAGTTA. qPCR analysis of pigeon tissues was performed on 384-well plates in a total volume of 10 µl, whereas our laser dissection studies and time course experiments used 96-well plates with 20-µl volumes. To maximize the accuracy of the qPCR results, three internal control genes (*clHPRT*, *clGAPDH*, and *clTFRC*) were included on each plate, together with no template controls for each primer set. Gene expression was calculated relative to the geometric mean of the three control genes. All experiments were conducted in accordance with the prescribed regulatory directives (Magistrat 60, Veterinäramt, MA60-001603/2010/002; Magistratsabteilung 58, GZ: 214635/2015/20).

Laser microdissection

For laser microdissection, adult pigeons (*n* = 3) were euthanized at approximately midday. The retinas were extracted under ribonuclease (RNase)–free conditions in a 4°C cold room using DEPC (Diethyl pyrocarbonate)–treated 1× phosphate-buffered saline (PBS). For each bird, the right eye was removed and hemisected, and the central region of the retina was isolated in less than 10 min. The retina was directly snap-frozen in optimal cutting temperature medium on dry ice (without cryoprotection in sucrose solution) and stored at −80°C. Frozen sections (10 µm) were cut with a cryostat at −20°C and mounted on RNase-free polyethylene naphthalate membrane

slides (Leica Microsystems, 11505189). The sections were fixed in 70% ethanol, stained with Mayer's hematoxylin (Sigma-Aldrich, MHS32), and dehydrated in 100% ethanol. The dehydrated slides were kept on dry ice until laser microdissection. For each slide, 20 pieces of a single layer were microdissected within 30 min (×40 magnification) and collected into the cap of a 0.5-μl tube containing 35 μl of TRIzol lysis buffer (Thermo Fisher Scientific, 15596026). The microdissected samples were snap-frozen in liquid nitrogen and stored at −80°C. The RNA was isolated by chloroform extraction and purified from the aqueous phase using the RNA Clean & Concentrator Kit (Zymo Research, R1015). Equal amounts of eluted RNA were pooled for the three birds and reverse-transcribed to generate cDNA (Qiagen, 205314).

Antibody generation

A C-terminal polypeptide unique to clCRY4 was selected as the antigen (H405-E525) for antibody generation. A codon-optimized transcript including an N-terminal His tag was synthesized and cloned into the pET14b expression vector (GenScript USA). The peptide was recombinantly expressed in bacteria (New England Biolabs, C2528J) and purified from bacterial lysates with a nickel-Sepharose column (GE Healthcare, 17526801) and the Whatman Elutrap electroelution system (Thermo Fisher Scientific, 15560753). BALB/c mice were immunized with this antigen, and monoclonal antibodies were produced using the hybridoma technique. The HAT (hypoxanthine-aminopterin-thymidine) selection system was used to select for fused hybridomas, and the surviving cells were seeded in multiwell plates. The hybridoma supernatants were screened by Western blot using lysates of chicken embryonic fibroblasts transiently transfected with GFP-tagged clCRY4. Positive wells were selected for monoclonalization by minimal dilution to obtain hybridoma clones originating from a single cell. To obtain high yields of monoclonal antibodies, the cells were first weaned off the selection media and then seeded into 350-ml bioreactor flasks (Sigma-Aldrich, Z688037-5EA), allowing subsequent harvests of supernatants containing high levels of secreted antibodies. To avoid contamination with bovine immunoglobulin Gs (IgGs) present in standard fetal bovine serum (FBS), purified FBS with IgG levels <5 μg/ml was used (Gibco, A3381901). The bioreactor supernatants were purified in a final step using a gravity-flow protein G column (GE Healthcare, 28-9852-55), and the purified antibodies were quantified by NanoDrop 2000 and stored at −20°C.

Antibody validation by Western blot analysis

GFP-tagged recombinant cryptochromes (GFP-clCRY1a, GFP-clCRY1b, GFP-clCRY2a, GFP-clCRY2b, and GFP-clCRY4) were expressed in pigeon embryonic fibroblasts (PEFs) using the pCIneo mammalian expression vector (Promega, E1841). PEFs were cultured in Dulbecco's modified Eagle's medium (DMEM), supplemented with 1% penicillin-streptomycin (Sigma-Aldrich, P0781), 1% L-glutamine (Sigma-Aldrich, G7513), 1% nonessential amino acids (Sigma-Aldrich, M7145), 0.5% sodium pyruvate (Sigma-Aldrich, S8636), 70 mM β-mercaptoethanol, 6% FBS (Gibco, 10270-106), and 8% chicken serum (Sigma-Aldrich, C5405). To transfect a 10-cm dish, 20 μg of plasmid and 30 μl of Lipofectamine 2000 transfection reagent (Invitrogen, 11668) were diluted in Opti-MEM reduced serum medium (Gibco, 31985070) according to the manufacturer's instructions. After 24 hours, the transiently transfected cells were washed with PBS and pelleted following trypsinization. The cell pellet was snap-frozen in liquid N_2. Cells were then lysed in radioimmunoprecipitation assay buffer [150 mM NaCl, 1% Triton X-100, 0.5% sodium deoxycholate, 0.1% SDS, and 50 mM tris (pH 8.0)] by pipetting, incubated at 4°C for 1 hour, and centrifuged for 30 min at 4°C (16,200*g*). The supernatant was collected and stored at −80°C until use. Protein concentration was determined using the detergent-compatible BCA assay (Thermo Fisher Scientific, 23225). For SDS-PAGE, 20 μg of protein was denatured by heat (95°C, 3 to 5 min) and loaded into the wells of a precast 15-well 7.5% tris-glycine polyacrylamide gel (Bio-Rad, 4568026). The gel was run at constant 80 to 100 V using tris-glycine electrophoresis buffer (Bio-Rad, 1610732), and the proteins were transferred onto nitrocellulose membranes by wet electroblotting overnight at constant 30 mA at 4°C. Membranes were stained with Ponceau S to confirm transfer, destained in ultra-pure, sterile H_2O (ddH_2O), and blocked for 1 hour in 5% milk tris-buffered saline with 0.1% Tween (TBST). clCRY4 antibodies (2 μg/ml) were incubated for 2 hours at room temperature (RT) in TBST buffer while shaking, in the presence or absence of the antigen (10-fold excess by mass) used for immunization. His-beads (5%, v/v; Invitrogen, 10103D) were added for 10 min at RT while shaking; the beads were pelleted, and the supernatant was supplemented with 10% milk-TBST for a final concentration of 1 μg/ml CRY4 antibody in 5% milk-TBST. The primary clCRY4 antibodies were added to the membranes and incubated overnight at 4°C under gentle agitation. As a control, a rabbit GFP antibody (Abcam, 6556) was used 1:2000 in 5% milk-TBST. Membranes were washed three times in TBST for 10 min each and incubated for 1 hour with the horseradish peroxidase (HRP)–tagged anti-rabbit or anti-mouse secondary antibody diluted 1:10,000 or 1:5000 in 0.5% milk-PBST (Abcam, ab6721, ab6823). To confirm that our clCRY4 antibodies do not cross-react with GRIP1 and GRIP2, Neuro2A cells were transfected with 10 μg of a plasmid (pCINeo) expressing MYC-CRY4, GRIP1-FLAG or GRIP-FLAG. Cells were harvested 48 hours later using ice-cold PBS, pelleted, and lysed for 1 hour using ice-cold lysis buffer. Each lysate was quantified using a BCA assay (Pierce BCA Protein Assay Kit, 23225) and 10 μg of lysate loaded on a NuPAGE 4 to 12% Bis-Tris Protein Gels (Invitrogen, NP0323BOX) before transfer onto a nitrocellulose membrane (GE Healthcare, 10600002). The membrane was cut vertically into three parts and probed with either a goat polyclonal FLAG antibody (Abcam, Ab1257, 1:10000), 7C11 clCRY4 (1 μg/ml), or 2B5 clCRY4 (1 μg/ml) diluted in 2.5% milk-TBST overnight at 4°C. Membranes were washed before application of the appropriate secondary antibody rabbit α-goat for 1 hour in 2.5% milk-TBST (Abcam, Ab6741, 1:10000) or goat α-mouse (Abcam, Ab6823, 1:5000). For detection, membranes were washed three times and incubated with the chemiluminescent detection reagents. The ECL Western blotting detection reagents (Amersham, RPN2106) were mixed in equal volume and supplemented with ECL select detection reagents (Amersham, RPN2235) in a 10:1 ratio to enhance signal intensity. The membrane was incubated with the blotting reagents for 90 s, excess fluid was removed, and the chemiluminescent signal was imaged on a ChemiDoc Touch system.

Immunohistochemistry

Pigeons were euthanized (n = 10), and the retina was dissected before fixation in 4% phosphate-buffered paraformaldehyde for a period of 20 min. Following dehydration in 30% sucrose, the retina was embedded in Neg-50 frozen section medium (Thermo Fisher Scientific, 6502), and 12-μm sections were prepared. Before immunostaining, sections were dried overnight and subject to antigen retrieval

by heating gradually to 90°C over 1 hour in antigen retrieval buffer (Vector, H-3301). For permanent staining, sections were incubated overnight at RT in a humidified chamber with the primary antibody (1:500) in 0.3% Triton X-100/PBS supplemented with 4% dry milk powder. Sections were then washed in 3× PBS for 5 min and incubated with the HRP-tagged secondary antibody for 1 hour (Vector, MP-7402), before visualization with VIP purple (Vector, SK-4600). For fluorescent staining, sections were incubated with the primary antibody overnight at RT in a humidified chamber in 0.3% Triton X-100/PBS supplemented with 2% donkey serum (abcam, ab7475). The following concentrations were used: clCRY4 2B5, 1:500 (7.2 μg/ml); clCRY4 7C11, 1:500 (7.5 μg/ml); GRIP2, 1:500 (Abcam, ab177891); and calretinin, 1:500 (Swant, CR-7697). The next day, sections were washed three times with PBS for 5 min and exposed to fluorescently conjugated secondary antibodies [donkey anti-mouse 488 (Thermo Fisher Scientific, A21202) 1:500; donkey anti-rabbit 568 (Thermo Fisher Scientific, A10042) 1:500] for 1 hour. Sections were counterstained with 4′,6-diamidino-2-phenylindole (1:1000, Thermo Fisher Scientific, H3569) before mounting (Dako, S3023). Images were captured on a Zeiss 710 confocal microscope at various magnifications.

Coimmunoprecipitation

To precipitate clCRY4 and its interacting partners, Dynabeads coupled to protein G (Life Technologies, 10003D) were equilibrated in two washes of 500 μl of 0.04% Triton X-100/TBS [20 mM tris (pH 7.5) and 150 mM NaCl]. Purified clCRY4 antibody (20 μg) was added to 100 μl of Protein G beads in 500 μl of TBST for 1 hour while rotating to bind the antibody to the beads. Unbound antibody was removed by three washes in 500 μl of Triton X-100/TBS (5 min each). For covalent cross-linking, the antibody-bead complex was washed briefly three times in 500 μl of 0.2 M sodium borate (pH 9.2) and mixed for 30 min with 1 ml of 20 mM dimethyl pimelimidate (prepared fresh in 0.2 M sodium borate solution). Antibody beads were washed twice for 10 min with 500 μl of 0.2 M tris-HCl (pH 8.0), twice briefly with 500 μl of Triton X-100/TBS, and twice more with 500 μl of 0.1 M glycine (pH 2.0). Last, the beads were washed three times with 500 μl of Triton X-100/TBS. Snap-frozen pigeon tissue samples harvested at midday (11:30 a.m. to 12:30 p.m.) were homogenized in lysis buffer [20 mM tris (pH 7.5), 100 mM NaCl, 10% glycerol, 1% Triton X-100, and protease inhibitor tablet], for 2 min at 20 Hz (30 Hz for liver) (TissueLyser, Qiagen). Lysates were initially transferred to antibody-free beads and incubated for 1 hour with rotation to allow nonspecific binding. Lysates were then transferred to either clCRY4 (sample) of GFP (control) antibody-coupled beads. Samples were incubated for 30 min with rotation, the supernatant was removed, and the beads were washed five times with 800 μl of wash buffer to remove unspecific proteins [20 mM tris (pH 7.5), 150 mM NaCl, 10% glycerol, 2 mM EDTA, 0.1% NP-40, and protease inhibitor tablet]. To remove detergents, the beads were washed 10 times with 800 μl of TBS [20 mM tris (pH 7.5) and 150 mM NaCl], and washed two final times with 800 ml of 150 mM NaCl. All steps with samples were performed at 4°C. The bead pellet was stored dry at −80°C until mass spectrometric analysis.

Mass spectrometry

Samples were processed by on-bead digest with Lys-C and glycine protease before they were reduced, alkylated, and digested with trypsin. For separation of the protein samples, the high-performance liquid chromatography system Dionex UltiMate 3000 RSLCnano (Thermo Fisher Scientific) was used coupled to a Q Exactive mass spectrometer (Thermo Fisher Scientific), equipped with a Proxeon nanospray source. Peptides were loaded onto a trap column (Thermo Fisher Scientific, PepMap C18; length, 5 mm; diameter, 300 μm; particle size, 5 μm; pore size, 100 Å) at a flow rate of 25 μl/min using 0.1% trifluoroacetic acid as a mobile phase. After 10 min, the trap column was switched in line with the analytical column (Thermo Fisher Scientific, PepMap C18; length, 500 mm, diameter, 75 μm, particle size, 2 μm, pore size, 100 Å). Peptides were eluted using a flow rate of 230 nl/min, and a binary 3-hour gradient. The solvent gradient used the mobile phases A (H_2O/formic acid, 99.9/0.1%, v/v) and B (H_2O/acetonitrile/formic acid, 19.92/80/0.08%), starting with 98% A and 2% B, increasing to 35% B over 180 min, followed by an increase to 90% B over 5 min, remaining at 90% B for 5 min, and decreasing back to 98% A and 2% B over 5 min. The Q Exactive HF mass spectrometer was operated in the data-dependent mode, using a full scan (mass/charge ratio range of 380 to 1500 and nominal resolution of 60,000), followed by tandem mass spectrometry (MS/MS) scans of the 10 most abundant ions. For peptide identification, the files were loaded into the Proteome Discoverer software (Thermo Fisher Scientific, version 2.1.0.81), and the created MS/MS spectra were searched against the National Center for Biotechnology Information (NCBI) pigeon genome. The peptide mass tolerance was set to ±5 ppm and the fragment mass tolerance was set to ±30 mmu. The maximal number of missed cleavages was set to 2, and the result was filtered to 1% false discovery rate at the peptide level. To control for nonspecific binding of proteins to monoclonal antibodies, we excluded those peptides that were identified when precipitating with GFP.

Validation of interacting partners

Neuro2A cells were cultured in DMEM and 10% FBS (Sigma-Aldrich, F7524), 1% penicillin/streptomycin (Gibco, 15070063), 1% L-glutamine (Gibco, 25030081), and 1% nonessential amino acids (Gibco, 11140050). Cells were cotransfected with 10 μg of an N-terminally MYC-tagged clCRY4 expression construct (pCINeo:MYC-clCRY4) and 10 μg of an expression construct containing open reading frames of potential clCRY4 interactors with a (C)-terminal FLAG tag sequence (pCIneo: Putative Interactor-FLAG). Transfection was performed using Lipofectamine 2000 (Invitrogen, 11668030) and Opti-MEM (Gibco, 31985062). Four hours after transfection, transfection reagents were aspirated and replaced with Neuro2A cell culture medium. Cells were incubated for 24 hours before harvesting in ice-cold PBS, pelleted by centrifugation, and lysed with ice-cold lysis buffer [20 mM tris-HCl (pH 7.5), 100 mM NaCl, 10% glycerol, 1% Triton X-100, and 1% Halt Protease and Phosphatase Inhibitor Cocktail, Thermo Fisher Scientific, 1861281] for 1 hour, on ice. Cell lysates were obtained by centrifugation, and total protein content was quantified (Pierce BCA Protein Assay Kit, Thermo Fisher Scientific, 23225). One microgram of cell lysate was then incubated with 40 μl of anti-FLAG M2 magnetic beads (Sigma-Aldrich, M8823) at 4°C for 2.5, with constant rotation. Using a magnetic rack, FLAG-tagged magnetic beads were pelleted, and the supernatant was aspirated and then washed five times with 800 μl of ice-cold wash buffer [20 mM tris-HCl (pH 7.5), 150 mM NaCl, 2 mM EDTA, 10% glycerol, 0.1% NP-40, and 1% Halt Protease and Phosphatase Inhibitor Cocktail], rotating at 4°C for 5 min. Proteins of interest were eluted with 50 μl of 3xFLAG peptide (0.3 mg/ml; Bachem, 4046200) diluted in Triton X-100/TBS, rotating, at 4°C for 30 min. Lysates (inputs) and eluates

were run on NuPAGE 4 to 12% Bis-Tris Protein Gels (Invitrogen, NP0323BOX) and transferred to nitrocellulose membranes (GE Healthcare, 10600002). Membranes were immunostained using a MYC monoclonal (produced in house, 1:200) or goat polyclonal α-FLAG (Abcam, Ab1257, 1:10,000) before probing with HRP-tagged secondaries: goat α-mouse (Abcam, ab6823, 1:5000) and rabbit α-goat (Abcam, ab6741, 1:10,000). Membranes were developed using ECL Select Western Blotting Detection Reagent (GE Healthcare, RPN2235).

SUPPLEMENTARY MATERIALS

Supplementary material for this article is available at http://advances.sciencemag.org/cgi/content/full/6/33/eabb9110/DC1

View/request a protocol for this paper from *Bio-protocol*.

REFERENCES AND NOTES

1. S. Johnsen, K. J. Lohmann, The physics and neurobiology of magnetoreception. *Nat. Rev. Neurosci.* **6**, 703–712 (2005).
2. T. Ritz, S. Adem, K. Schulten, A model for photoreceptor-based magnetoreception in birds. *Biophys. J.* **78**, 707–718 (2000).
3. P. J. Hore, H. Mouritsen, The radical-pair mechanism of magnetoreception. *Annu. Rev. Biophys.* **45**, 299–344 (2016).
4. W. Wiltschko, R. Wiltschko, Light-dependent magnetoreception in birds: The behaviour of European robins, Erithacus rubecula, under monochromatic light of various wavelengths and intensities. *J. Exp. Biol.* **204**, 3295–3302 (2001).
5. J. B. Phillips, S. C. Borland, Behavioural evidence for use of a light-dependent magnetoreception mechanism by a vertebrate. *Nature* **359**, 142–144 (1992).
6. R. J. Gegear, A. Casselman, S. Waddell, S. M. Reppert, Cryptochrome mediates light-dependent magnetosensitivity in Drosophila. *Nature* **454**, 1014–1018 (2008).
7. R. A. W. Wiltschko, Pigeon homing: Effect of various wavelengths of light during displacement. *Naturwissenschaften* **85**, 164–167 (1998).
8. S. Engels, N. L. Schneider, N. Lefeldt, C. M. Hein, M. Zapka, A. Michalik, D. Elbers, A. Kittel, P. J. Hore, H. Mouritsen, Anthropogenic electromagnetic noise disrupts magnetic compass orientation in a migratory bird. *Nature* **509**, 353–356 (2014).
9. T. Ritz, P. Thalau, J. B. Phillips, R. Wiltschko, W. Wiltschko, Resonance effects indicate a radical-pair mechanism for avian magnetic compass. *Nature* **429**, 177–180 (2004).
10. A. Pinzon-Rodriguez, R. Muheim, Zebra finches have a light-dependent magnetic compass similar to migratory birds. *J. Exp. Biol.* **220**, 1202–1209 (2017).
11. E. P. Malkemper, S. H. Eder, S. Begall, J. B. Phillips, M. Winklhofer, V. Hart, H. Burda, Magnetoreception in the wood mouse (*Apodemus sylvaticus*): Influence of weak frequency-modulated radio frequency fields. *Sci. Rep.* **4**, 9917 (2015).
12. M. Vacha, T. Puzova, M. Kvicalova, Radio frequency magnetic fields disrupt magnetoreception in American cockroach. *J. Exp. Biol.* **212**, 3473–3477 (2009).
13. I. Chaves, R. Pokorny, M. Byrdin, N. Hoang, T. Ritz, K. Brettel, L. O. Essen, G. T. van der Horst, A. Batschauer, M. Ahmad, The cryptochromes: Blue light photoreceptors in plants and animals. *Annu. Rev. Plant Biol.* **62**, 335–364 (2011).
14. K. Koh, X. Zheng, A. Sehgal, JETLAG resets the Drosophila circadian clock by promoting light-induced degradation of TIMELESS. *Science* **312**, 1809–1812 (2006).
15. C. L. Partch, C. B. Green, J. S. Takahashi, Molecular architecture of the mammalian circadian clock. *Trends Cell Biol.* **24**, 90–99 (2014).
16. R. J. Kutta, N. Archipowa, L. O. Johannissen, A. R. Jones, N. S. Scrutton, Vertebrate cryptochromes are vestigial flavoproteins. *Sci. Rep.* **7**, 44906 (2017).
17. A. Czarna, A. Berndt, H. R. Singh, A. Grudziecki, A. G. Ladurner, G. Timinszky, A. Kramer, E. Wolf, Structures of Drosophila cryptochrome and mouse cryptochrome1 provide insight into circadian function. *Cell* **153**, 1394–1405 (2013).
18. C. T. Rodgers, P. J. Hore, Chemical magnetoreception in birds: The radical pair mechanism. *Proc. Natl. Acad. Sci. U.S.A.* **106**, 353–360 (2009).
19. D. Nohr, S. Franz, R. Rodriguez, B. Paulus, L. O. Essen, S. Weber, E. Schleicher, Extended electron-transfer in animal cryptochromes mediated by a tetrad of aromatic amino acids. *Biophys. J.* **111**, 301–311 (2016).
20. B. D. Zoltowski, Y. Chelliah, A. Wickramaratne, L. Jarocha, N. Karki, W. Xu, H. Mouritsen, P. J. Hore, R. E. Hibbs, C. B. Green, J. S. Takahashi, Chemical and structural analysis of a photoactive vertebrate cryptochrome from pigeon. *Proc. Natl. Acad. Sci. U.S.A.* **116**, 19449–19457 (2019).
21. S. Weber, T. Biskup, A. Okafuji, A. R. Marino, T. Berthold, G. Link, K. Hitomi, E. D. Getzoff, E. Schleicher, J. R. Norris Jr., Origin of light-induced spin-correlated radical pairs in cryptochrome. *J. Phys. Chem. B* **114**, 14745–14754 (2010).
22. D. Nohr, B. Paulus, R. Rodriguez, A. Okafuji, R. Bittl, E. Schleicher, S. Weber, Determination of radical-radical distances in light-active proteins and their implication for biological magnetoreception. *Angew. Chem.* **56**, 8550–8554 (2017).
23. S. Haverkamp, U. Grunert, H. Wassle, The cone pedicle, a complex synapse in the retina. *Neuron* **27**, 85–95 (2000).
24. A. J. Fischer, J. J. Stanke, G. Aloisio, H. Hoy, W. K. Stell, Heterogeneity of horizontal cells in the chicken retina. *J. Comp. Neurol.* **500**, 1154–1171 (2007).
25. C. Holt, M. Campbell, D. A. Keays, N. Edelman, A. Kapusta, E. Maclary, E. T. Domyan, A. Suh, W. C. Warren, M. Yandell, M. T. P. Gilbert, M. D. Shapiro, Improved genome assembly and annotation for the rock pigeon (*Columba livia*). *G3* **8**, 1391–1398 (2018).
26. H. Dong, R. J. O'Brien, E. T. Fung, A. A. Lanahan, P. F. Worley, R. L. Huganir, GRIP: A synaptic PDZ domain-containing protein that interacts with AMPA receptors. *Nature* **386**, 279–284 (1997).
27. H. Dong, P. Zhang, I. Song, R. S. Petralia, D. Liao, R. L. Huganir, Characterization of the glutamate receptor-interacting proteins GRIP1 and GRIP2. *J. Neurosci.* **19**, 6930–6941 (1999).
28. R. Gabriel, S. de Souza, E. B. Ziff, P. Witkovsky, Association of the AMPA receptor-related postsynaptic density proteins GRIP and ABP with subsets of glutamate-sensitive neurons in the rat retina. *J. Comp. Neurol.* **449**, 129–140 (2002).
29. X. Wang, C. Jing, C. P. Selby, Y. Y. Chiou, Y. Yang, W. Wu, A. Sancar, J. Wang, Comparative properties and functions of type 2 and type 4 pigeon cryptochromes. *Cell. Mol. Life Sci.* **75**, 4629–4641 (2018).
30. O. Berntsson, R. Rodriguez, L. Henry, M. R. Panman, A. J. Hughes, C. Einholz, S. Weber, J. A. Ihalainen, R. Henning, I. Kosheleva, E. Schleicher, S. Westenhoff, Photoactivation of *Drosophila melanogaster* cryptochrome through sequential conformational transitions. *Sci. Adv.* **5**, eaaw1531 (2019).
31. S. Franz, E. Ignatz, S. Wenzel, H. Zielosko, E. P. G. N. Putu, M. Maestre-Reyna, M.-D. Tsai, J. Yamamoto, M. Mittag, L.-O. Essen, Structure of the bifunctional cryptochrome aCRY from *Chlamydomonas reinhardtii*. *Nucleic Acids Res.* **46**, 8010–8022 (2018).
32. A. Czarna, A. Berndt, H. R. Singh, A. Grudziecki, A. G. Ladurner, G. Timinszky, A. Kramer, E. Wolf, Structures of *Drosophila* cryptochrome and mouse cryptochrome1 provide insight into circadian function. *Cell* **153**, 1394–1405 (2013).
33. B. D. Zoltowski, Y. Chelliah, A. Wickramaratne, L. Jarocha, N. Karki, W. Xu, H. Mouritsen, P. J. Hore, R. E. Hibbs, C. B. Green, J. S. Takahashi, Chemical and structural analysis of a photoactive vertebrate cryptochrome from pigeon. *Proc. Natl. Acad. Sci. U.S.A.* **116**, 19449–19457 (2019).
34. A. Pinzon-Rodriguez, S. Bensch, R. Muheim, Expression patterns of cryptochrome genes in avian retina suggest involvement of Cry4 in light-dependent magnetoreception. *J. R. Soc. Interface* **15**, 20180058 (2018).
35. A. Günther, A. Einwich, E. Sjulstok, R. Feederle, P. Bolte, K. W. Koch, I. A. Solov'yov, H. Mouritsen, Double-cone localization and seasonal expression pattern suggest a role in magnetoreception for European Robin Cryptochrome 4. *Curr. Biol.* **28**, 211–223.e4 (2018).
36. R. Watari, C. Yamaguchi, W. Zemba, Y. Kubo, K. Okano, T. Okano, Light-dependent structural change of chicken retinal Cryptochrome4. *J. Biol. Chem.* **287**, 42634–42641 (2012).
37. Y. Kubo, M. Akiyama, Y. Fukada, T. Okano, Molecular cloning, mRNA expression, and immunocytochemical localization of a putative blue-light photoreceptor CRY4 in the chicken pineal gland. *J. Neurochem.* **97**, 1155–1165 (2006).
38. A. P. Mariani, Neuronal and synaptic organization of the outer plexiform layer of the pigeon retina. *Am. J. Anat.* **179**, 25–39 (1987).
39. M. Han, R. Mejias, S. L. Chiu, R. Rose, A. Adamczyk, R. Huganir, T. Wang, Mice lacking GRIP1/2 show increased social interactions and enhanced phosphorylation at GluA2-S880. *Behav. Brain Res.* **321**, 176–184 (2017).
40. K. Takamiya, L. Mao, R. L. Huganir, D. J. Linden, The glutamate receptor-interacting protein family of GluR2-binding proteins is required for long-term synaptic depression expression in cerebellar Purkinje cells. *J. Neurosci.* **28**, 5752–5755 (2008).
41. R. Mejias, S. L. Chiu, M. Han, R. Rose, A. Gil-Infante, Y. Zhao, R. L. Huganir, T. Wang, Purkinje cell-specific Grip1/2 knockout mice show increased repetitive self-grooming and enhanced mGluR5 signaling in cerebellum. *Neurobiol. Dis.* **132**, 104602 (2019).
42. K. J. Fogle, K. G. Parson, N. A. Dahm, T. C. Holmes, CRYPTOCHROME is a blue-light sensor that regulates neuronal firing rate. *Science* **331**, 1409–1413 (2011).
43. L. S. Baik, K. J. Fogle, L. Roberts, A. M. Galschiodt, J. A. Chevez, Y. Recinos, V. Nguy, T. C. Holmes, CRYPTOCHROME mediates behavioral executive choice in response to UV light. *Proc. Natl. Acad. Sci. U.S.A.* **114**, 776–781 (2017).
44. A. Odeen, O. Hastad, The phylogenetic distribution of ultraviolet sensitivity in birds. *BMC Evol. Biol.* **13**, 36 (2013).
45. N. G. Nimpf, S. Kagerbauer, D. Malkemper, E. P. Landler, L. Papadaki-Anastasopoulou, A. Ushakova, L. Wenninger-Weinzierl, A. Novatchkova, M. Vincent, P. Lendl, T. Colombini, M. Mason, M. J. Keays, A putative mechanism for magnetoreception by electromagnetic induction in the pigeon inner ear. *Curr. Biol.* **29**, 4052–4059.e4 (2019).
46. B. Paulus, C. Bajzath, F. Melin, L. Heidinger, V. Kromm, C. Herkersdorf, U. Benz, L. Mann, P. Stehle, P. Hellwig, S. Weber, E. Schleicher, Spectroscopic characterization of radicals

and radical pairs in fruit fly cryptochrome—Protonated and nonprotonated flavin radical-states. *FEBS J.* **282**, 3175–3189 (2015).
47. K. M. Salikhov, Y. E. Kandrashkin, A. K. Salikhov, Peculiarities of free induction and primary spin echo signals for spin-correlated radical pairs. *Appl. Magn. Reson.* **3**, 199–216 (1992).
48. C. E. Fursman, P. J. Hore, Distance determination in spin-correlated radical pairs in photosynthetic reaction centres by electron spin echo envelope modulation. *Chem. Phys. Letters* **303**, 593–600 (1999).
49. A. Okafuji, A. Schnegg, E. Schleicher, K. Mobius, S. Weber, G-tensors of the flavin adenine dinucleotide radicals in glucose oxidase: A comparative multifrequency electron paramagnetic resonance and electron-nuclear double resonance study. *J. Phys. Chem. B* **112**, 3568–3574 (2008).
50. G. Bleifuss, M. Kolberg, S. Potsch, W. Hofbauer, R. Bittl, W. Lubitz, A. Graslund, G. Lassmann, F. Lendzian, Tryptophan and tyrosine radicals in ribonucleotide reductase: A comparative high-field EPR study at 94 GHz. *Biochemistry* **40**, 15362–15368 (2001).
51. R. Pogni, M. C. Baratto, C. Teutloff, S. Giansanti, F. J. Ruiz-Duenas, T. Choinowski, K. Piontek, A. T. Martinez, F. Lendzian, R. Basosi, A tryptophan neutral radical in the oxidized state of versatile peroxidase from *Pleurotus eryngii*. *J. Biol. Chem.* **281**, 9517–9526 (2006).
52. C. Levy, B. D. Zoltowski, A. R. Jones, A. T. Vaidya, D. Top, J. Widom, M. W. Young, N. S. Scrutton, B. R. Crane, D. Leys, Updated structure of Drosophila cryptochrome. *Nature* **495**, E3–E4 (2013).
53. S. Franz, E. Ignatz, S. Wenzel, H. Zielosko, E. Putu, M. Maestre-Reyna, M. D. Tsai, J. Yamamoto, M. Mittag, L.-O. Essen, Structure of the bifunctional cryptochrome aCRY from *Chlamydomonas reinhardtii*. *Nucleic Acids Res.* **46**, 8010–8022 (2018).

Acknowledgments: We wish to thank the scientific services at the Research Institute for Molecular Pathology and the Vienna Biocenter Core Facilities (VBCF), particularly A. Sedivy.

Funding: D.A.K. was supported by the European Research Council (ERC, 336725, 819336) and the FWF (Y726). S.N. is a recipient of a DOC Fellowship of the Austrian Academy of Sciences. L.L. was supported by the FWF (P32586). S.W. and E.S. thank the SIBW/DFG for financing EPR instrumentation at the University of Freiburg and the DFG (235777276/GRK1976) for financial support. K.M. was financed by the EPIC-XS initiative (823839), the Horizon 2020 Program, and by the Austrian Science Fund (I 3686). **Author contributions:** Conceptualization: T.H. and D.A.K.. Investigation: T.H., T.A.S., D.M., F.W., A.V., M.P., T.D.C., W.S., S.N., G.C.N., N.E., L.K., E.P.M., G.D., S.W., and D.A.K. Formal analysis: T.H., T.A.S., D.A.K., L.L., S.W., and E.S. Resources: T.A.S., E.O., S.S., and E.S. Writing of original draft: D.A.K.. Writing, reviewing, and editing: T.H., T.A.S., D.M., F.W., A.V., T.D.C., W.S., S.N., G.C.N., N.E., E.P.M., S.W., and E.S. Funding acquisition: E.S. and D.A.K.. Supervision: E.S., K.M., and D.A.K. **Competing interests:** The authors declare that they have no competing interests. **Data and materials availability:** All data needed to evaluate the conclusions in the paper are present in the paper and/or the Supplementary Materials. Additional data related to this paper may be requested from the authors. The mRNA sequences of the pigeon cryptochromes have been submitted to the NCBI GenBank database and can be retrieved using the following accession numbers: KX168607 (*clCRY1a*), KX168608 (*clCRY1b*), KX168609 (*clCRY2a*), KX168610 (*clCRY2b*), and KX168611 (*clCRY4*).

Submitted 26 March 2020
Accepted 26 June 2020
Published 12 August 2020
10.1126/sciadv.abb9110

Citation: T. Hochstoeger, T. Al Said, D. Maestre, F. Walter, A. Vilceanu, M. Pedron, T. D. Cushion, W. Snider, S. Nimpf, G. C. Nordmann, L. Landler, N. Edelman, L. Kruppa, G. Dürnberger, K. Mechtler, S. Schuechner, E. Ogris, E. P. Malkemper, S. Weber, E. Schleicher, D. A. Keays, The biophysical, molecular, and anatomical landscape of pigeon CRY4: A candidate light-based quantal magnetosensor. *Sci. Adv.* **6**, eabb9110 (2020).

The biophysical, molecular, and anatomical landscape of pigeon CRY4: A candidate light-based quantal magnetosensor

Tobias Hochstoeger, Tarek Al Said, Dante Maestre, Florian Walter, Alexandra Vilceanu, Miriam Pedron, Thomas D. Cushion, William Snider, Simon Nimpf, Gregory Charles Nordmann, Lukas Landler, Nathaniel Edelman, Lennard Kruppa, Gerhard Dürnberger, Karl Mechtler, Stefan Schuechner, Egon Ogris, E. Pascal Malkemper, Stefan Weber, Erik Schleicher and David A. Keays

Sci Adv **6** (33), eabb9110.
DOI: 10.1126/sciadv.abb9110